This document is the accepted manuscript version of the following article:
Vollmer, M. K., Mühle, J., Henne, S., Young, D., Rigby, M., Mitrevski, B., … Steele, L. P. (2021). Unexpected nascent atmospheric emissions of three ozone-depleting hydrochlorofluorocarbons. Proceedings of the National Academy of Sciences of the United States of America PNAS, 118(5), e2010914118 (7 pp.). https://doi.org/10.1073/pnas.2010914118

Unexpected nascent atmospheric emissions of three ozone-depleting hydrochlorofluorocarbons

Martin K. Vollmer[a,1], Jens Mühle[b], Stephan Henne[a], Dickon Young[c], Matthew Rigby[c], Blagoj Mitrevski[d], Sunyoung Park[e], Chris R. Lunder[f], Tae Siek Rhee[g], Christina M. Harth[b], Matthias Hill[a], Ray L. Langenfelds[d], Myriam Guillevic[a], Paul M. Schlauri[a], Ove Hermansen[f], Jgor Arduini[h,i], Ray H. J. Wang[j], Peter K. Salameh[b], Michela Maione[h,i], Paul B. Krummel[d], Stefan Reimann[a], Simon O'Doherty[c], Peter G. Simmonds[c], Paul J. Fraser[d], Ronald G. Prinn[k], Ray F. Weiss[b], and L. Paul Steele[d]

[a]Laboratory for Air Pollution and Environmental Technology, Empa, Swiss Federal Laboratories for Materials Science and Technology, Überlandstrasse 129, 8600 Dübendorf, Switzerland; [b]Scripps Institution of Oceanography, University of California, San Diego, La Jolla, California, USA.; [c]Atmospheric Chemistry Research Group, School of Chemistry, University of Bristol, Bristol, UK.; [d]Climate Science Centre, CSIRO Oceans and Atmosphere, Aspendale, Victoria, Australia.; [e]Kyungpook Institute of Oceanography, Kyungpook National University, South Korea.; [f]Norwegian Institute for Air Research, Kjeller, Norway.; [g]Korea Polar Research Institute (KOPRI), Incheon, South Korea.; [h]Department of Pure and Applied Sciences, University of Urbino, Urbino, Italy.; [i]Institute of Atmospheric Sciences and Climate, Italian National Research Council, Bologna, Italy.; [j]School of Earth and Atmospheric Sciences, Georgia Institute of Technology, Atlanta, Georgia, USA.; [k]Center for Global Change Science, Massachusetts Institute of Technology, Cambridge, Massachusetts, USA.

This manuscript was compiled on November 27, 2020

Global and regional atmospheric measurements and modeling can play key roles in discovering and quantifying unexpected nascent emissions of environmentally important substances. We focus here on three hydrochlorofluorocarbons that are restricted by the Montreal Protocol because of their roles in stratospheric ozone depletion. Based on measurements of archived air samples and on in situ measurements at stations of the Advanced Global Atmospheric Gases Experiment (AGAGE) network, we report global abundances, trends, and regional enhancements, for HCFC-132b ($CH_2ClCClF_2$), which is newly-discovered in the atmosphere, and updated results for HCFC-133a (CH_2ClCF_3) and HCFC-31 (CH_2ClF). No purposeful end-use is known for any of these compounds. We find that HCFC-132b appeared in the atmosphere 20 years ago and that its global emissions increased to 1.1 Gg yr^{-1} by 2019. Regional top-down emission estimates for East Asia, based on high-frequency measurements for 2016–2019, account for ∼95% of the global HCFC-132b emissions, and for ∼ 80% of the global HCFC-133a emissions of 2.3 Gg yr^{-1}, during this period. Global emissions of HCFC-31 for the same period are 0.71 Gg yr^{-1}. Small European emissions of HCFC-132b and HCFC-133a, found in southeastern France, ceased in early 2017 when a fluorocarbon production facility in that area closed. Although unreported emissive end-uses cannot be ruled out, all three compounds are most-likely emitted as intermediate byproducts in chemical production pathways. Identification of harmful emissions to the atmosphere at early stage can guide the effective development of global and regional environmental policy.

Montreal Protocol | Atmospheric Composition | Ozone Depletion

Localizing and quantifying halocarbon emissions from atmospheric observations and transport modelling has become an important tool to validate emissions derived from activity data and emission factors (1–7). This can also be used to detect new substances and derive their nascent trends and emissions, thereby playing an important role as an early warning system leading to improved environmental emissions policies.

Here we present long-term emissions of three ozone depleting substances (ODSs) which have no reported end-use. The emissive use of these substances is regulated by the Montreal Protocol on Substances that Deplete the Ozone Layer and its Amendments (hereafter referred to as the Montreal Protocol). The Montreal Protocol is an international agreement that regulates the phase-out of production and consumption of ODSs. The environmental target of these regulations is to lower ODS abundances in the atmosphere to safeguard the stratospheric ozone layer. The full ban on production and consumption for emissive end-use of the primary ODSs, the chlorofluorocarbons (CFCs), was set to the mid-1990s for developed (non-Article 5) countries and to 2010 globally. As a consequence, emissions have been declining when calculated based on production and consumption (bottom up). Unexpectedly though, emissions inferred from atmospheric observations (top-down method), of several ODSs were recently found to be declining more slowly than expected, or even increasing (4, 5, 8–10). This raised concerns about potential violations of the Montreal Protocol (4, 5, 11). However, it is difficult to prove a violation, because emissions are aggregated when using the top-down method, and additionally include those from banked ODSs in end-user products (e.g. refrigerators, foam), which are not controlled by the Montreal Protocol (12). Further, emissions from feedstock and process agents, and from inadvertent or coincidental production during a manufacturing process are also included into these aggregated top-down emission estimates. Although the Montreal Protocol addresses this group of emissions, no

Significance Statement

We demonstrate the need to detect and track unexpected substances in the atmosphere and to locate their sources. Here we report on three hydrochlorofluorocarbons that have no known end-uses. HCFC-132b ($CH_2ClCClF_2$) is newly discovered in the global atmosphere. We identify East Asia as the dominant source region for global emissions of this compound, and of HCFC-133a (CH_2ClCF_3). We also quantify global emissions of HCFC-31 (CH_2ClF). These compounds are most likely emitted as intermediate byproducts of chemical production processes. The early discovery and identification of such unexpected emissions can identify the related industrial practices, and help to develop and manage environmental policies to reduce unwanted and potentially harmful emissions before the scale of the problem becomes more costly to mitigate.

MKV, SR, RFW, PGS, PJF, RGP, SO, JM, LPS, PBK, BM, MM, SP designed the experiment, MKV, DY, JM, BM, CMH, CRL, TSR, OH, MH, PMS, MG, RLL, SO, LPS provided samples, calibrations and/or made the measurements, MR, SH made the model calculations, MKV wrote the article with contributions from all co-authors.

The authors declare no conflict of interest

[1]To whom correspondence should be addressed. E-mail: martin.vollmer@empa.ch

stringent control is enforced to date, with the Parties primarily being urged to take steps to minimize such emissions (11, 13, 14). Attention has so far been limited to only a small number of compounds, notably carbon tetrachloride (CCl_4), whose emissions are not declining as expected, partially due to unreported non-feedstock emissions (3, 15).

The three ODSs identified in this study are all hydrochlorofluorocarbons (HCFCs), which have lower potentials than CFCs to harm the ozone layer, and which have been used in the past as interim replacements for CFCs. Their phase-out by the Montreal Protocol was significantly tightened in 2007 with a complete ban in 2020 for developed (non-Article 5) countries and 2030 globally. HCFCs have also been included in the baseline calculations under the Kigali Amendment in 2016 to facilitate "leap-frogging" high global-warming-potential (GWP) hydrofluorocarbons (HFCs) by directly replacing HCFCs with low GWP substances (16, 17). Similar to the CFCs, the major HCFCs, HCFC-22 ($CHClF_2$), HCFC-142b (CH_3CClF_2), and HCFC-141b (CH_3CCl_2F), are used in stationary refrigeration and structural foam blowing. Their global emissions have leveled or started to decline over the past years as a consequence of their production phase-down (18).

We report on the newly detected HCFC-132b (1,2-dichloro-1,1-difluoroethane, $CH_2ClCClF_2$) in the atmosphere, and present substantial updates on abundance and emissions for the previously found HCFC-133a and HCFC-31 (8, 19, 20). Their lack of known end-uses gives rise to speculation about their sources and their roles within the framework of the Montreal Protocol. There are no public inventories or bottom-up emission reports available for these compounds. Although their physical and chemical properties are suitable for applications in refrigeration and other industrial applications, their toxicities and carcinogenicities have prevented consumer end-use applications in the past (21–25). Their removal from the atmosphere is mainly driven by reaction with the hydroxyl radical (OH), leading to global atmospheric lifetimes of 3.5 yr for HCFC-132b, 4.6 yr for HCFC-133a, and 1.2 yr for HCFC-31 (26).

The measurements presented here have wide geographical and temporal coverage, based on ongoing in situ ground-based measurements at the stations of the Advanced Global Atmospheric Gases Experiment (AGAGE) network (27). Our records also include measurements of archived air samples from the Southern Hemisphere (SH) Cape Grim Air Archive (CGAA) starting in 1978 and from the Northern Hemisphere (NH), as well as multi-year weekly collected air samples from Antarctica. We also extend the previous record of HCFC-133a with in situ AGAGE and new CGAA measurements (8, 19). Furthermore, we present a longer record for HCFC-31 than was previously available (20), through measurements of the CGAA, and updated contemporary observations from Antarctic samples (2015–2019) and NH measurements from Dübendorf (Switzerland).

Using these measurements, an inverse method, and the AGAGE 12-box atmospheric transport model, we estimate hemispheric emissions and reconstruct abundances of the three HCFCs from 1978 to the present (28, 29). Based on the large pollution events recorded at the AGAGE station, Gosan (Jeju Island, South Korea), we also estimate regional East Asian emissions of HCFC-132b and HCFC-133a using a regional inverse modeling system (30).

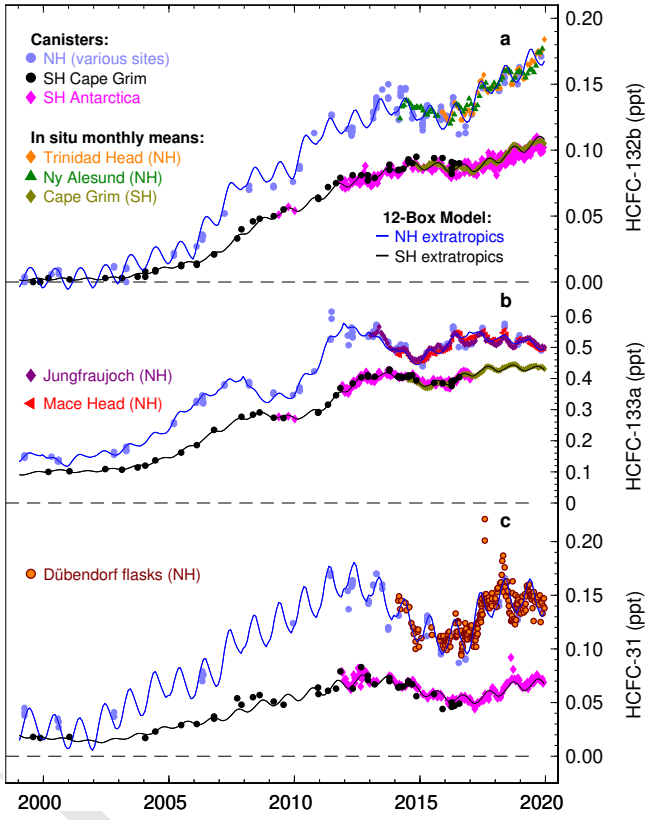

Fig. 1. Atmospheric observations and model reconstructions of the hydrochlorofluorocarbons (HCFCs), HCFC-132b (panel a), HCFC-133a (panel b), and HCFC-31 (panel c). Units are dry air mole fractions in ppt (pmol mol^{-1}). The ∼40 year long records are limited here to 1999–2019 for better temporal resolution. Flask sample results from various Northern Hemisphere sites are aggregated into a single data set for clarity. Flask samples for the Southern Hemisphere are shown for Cape Grim (Tasmania) and the Antarctic station King Sejong. In situ records for HCFC-132b and HCFC-133a from stations of the Advanced Global Atmospheric Gases Experiment (AGAGE) are shown here as background-filtered monthly means for a few illustrative stations only. Modeled records, derived from the observations and an inversion system using a 12-box chemical transport model, are shown for the four ground-level model boxes.

Results

Global Atmospheric Distributions of the HCFCs. We calculate hemispheric long-term trends by combining flask measurements with in situ high-resolution observations from AGAGE stations (Fig. 1). HCFC-132b first appeared in the NH atmosphere in the late 1990s followed by a sustained and rapid growth to a dry air mole fraction of 0.15 ppt (parts-per-trillion) by 2013 (Fig. 1a). After a short decline until 2016, the compound increased again to a maximum of 0.17 ppt by the end of 2019. The SH abundances lagged the NH abundances and remained lower throughout the entire record, indicating that emissions of this compound predominantly occurred in the NH. The absence of HCFC-132b from the atmosphere before 1995 (Supplement, not shown in Fig. 1a) suggests an entirely anthropogenic origin.

HCFC-133a exhibits a general increase in both hemispheres. Measurements of archived air from the US west coast detail a pronounced reversal in the NH abundance in 2007/2008, in agreement with a similar feature found for the SH (8). Also, independent measurements of the CGAA confirm earlier

findings, in particular the presence of this compound in the SH atmosphere before 1978 (8). New flask and in situ measurements for 2015–2019 reveal that the downward trend of HCFC-133a in the NH (2012–2015, (19)) has reversed and the compound has increased to >0.5 ppt again.

For HCFC-31, first detectable mole fractions appear in samples from the late 1990s. Following more than a decade-long growth, we find, similar to HCFC-133a, a decline of HCFC-31 in the atmosphere for 2012–2015, which was followed by another strong increase and a stabilization over the past 3 years.

There are surprising similarities in the records of the 3 compounds (Fig. 1). Compared to known records for many other halocarbons, we find large multi-year variability in these records, pointing to rapidly changing emissions. The most pronounced feature is a temporal maximum in abundances for all three compounds within the period 2012 – 2014, although not exactly synchronous.

Global Emissions. Global emissions for all three compounds show a generally increasing trend over the last two decades, with mean values for 2016–2019 of 0.97 Gg yr^{-1} for HCFC-132b, 2.3 Gg yr^{-1} for HCFC-133a, and 0.71 Gg yr^{-1} for HCFC-31 (Fig. 2). However, we calculate a large relative variability in these emissions, particularly for HCFC-133a. This variability is unusual compared to other widely used synthetic halocarbons (18) and indicates that a major fraction of these emissions does not originate from banks (compounds stored in equipment, which are usually emitted slowly over time and, hence, only exhibit small variability in their global emissions). It further suggests that the emissions are not deriving from impurities in commercially used halocarbons, which generally show temporally much smoother emission trends. Note that the emissions uncertainties in Fig. 2 are dominated by uncertainties in the lifetime, which act like potential biases across all years. Therefore, in our global inversions, the year-to-year variability is better constrained than the absolute emissions magnitude, particularly for HCFC-132b, which has a relatively large lifetime uncertainty.

Twenty-year cumulative emissions (1978 – 2019) for HCFC-132b, HCFC-133a, and HCFC-31 amount to 13 Gg, 44 Gg, and 10.6 Gg. Given their relatively small ozone depletion potentials (ODPs), compared to the primary ODSs, of 0.038, 0.019, and 0.019, respectively, (26), we calculate a combined cumulative emission of 1.5 Gg-ODP-weighted. Although their impacts on stratospheric ozone degradation are small and roughly one order of magnitude smaller compared to the recently found yearly unexpected emissions of CFC-11 (CCl_3F) (4, 5), their absolute emissions are significant, particularly for compounds with no purposeful end-use.

Emissions from East Asia. Within the AGAGE network, frequent and large (up to 4 ppt) pollution events for HCFC-132b and HCFC-133a were recorded at the South Korean station, Gosan, indicating substantial regional emissions (Fig. 3; HCFC-31 is not measured at the AGAGE sites, see Measurement Methods). By combining these records with an inverse modeling method (30), we find that the most concentrated emissions in East Asia (defined as China, Taiwan, North and South Korea, and Japan) occur in Eastern China (Fig. 2 and Fig. 4). For HCFC-132b, Eastern China emissions are 0.43 – 0.53 Gg yr^{-1} for 2016 – 2019 and account on average for 50% of global

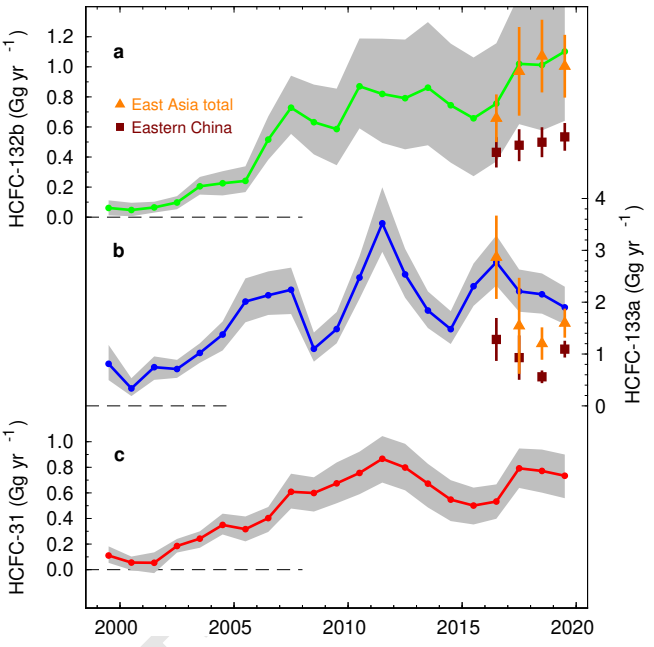

Fig. 2. Global and East Asia regional emissions of the hydrochlorofluorocarbons HCFC-132b (panel a), HCFC-133a (panel b), and HCFC-31 (panel c). Shaded grey bands denote the 16/84-percentile uncertainty range for the global emissions. Total emissions from East Asia (orange) and Eastern China only (maroon) are plotted for HCFC-132b and HCFC-133a with 95% confidence intervals (grey shading).

emissions (Fig. 2a). The East Asia total emissions account for ∼95% of the global emissions, within the uncertainties of the methods. The inversion attributes a large fraction of East Asian emissions to West China. However, due to the reduced sensitivity of the observational site to West China, these estimates are connected with a much larger uncertainty than for East China. For HCFC-133a, Eastern China emissions account on average for 43% of the global emissions, and East Asia emissions explain ∼80% of the global emissions (Fig. 2b).

There is a distinct difference in the geographical distribution of the emissions from Eastern China (Fig. 4). For HCFC-132b, the strongest source region is found in northeastern China (Shangdong and Southern Hebei). In contrast, for HCFC-133a the highest emissions are found in the Shanghai region. Both regions were recently identified as strong emitters of other halocarbons, but the predominance of HCFC-132b and HCFC-133a emissions to only one of these two regions is unusual (10, 31). Both areas host intense fluorocarbon industry, which could support speculations on feedstock/byproduct emissions. For CCl_4, another ODS with little-known allowed emissive end-uses, a study covering 2009–2016 found that emissions first originated in the Shanghai region but then spread out to include northern Chinese provinces (32). Recent similar high-emission regions were also found for CFC-11 with suggested ultimate emissive end-use (5).

Sources in Western Europe. We find much smaller and highly sporadic (2–3 times per year) pollution events for HCFC-132b (up to 0.5 ppt) and HCFC-133a (up to 3.5 ppt) at some of the European stations (mainly Jungfraujoch and Monte Cimone). Surprisingly, European pollution events for HCFC-132b ceased by early 2017 and those for HCFC-133a became even less frequent (see Supplement), indicating that regional

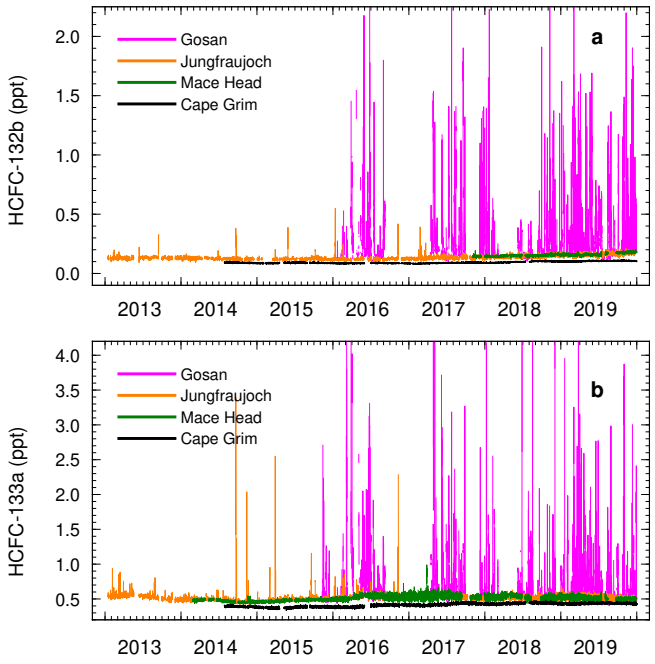

Fig. 3. High resolution measurement records of HCFC-132b (panel a) and HCFC-133a (panel b) from selected stations of the Advanced Global Atmospheric Gases Experiment (AGAGE). Pollution events recorded at the Gosan station (South Korea), where measurements started in 2015/2016, strongly exceed those at all other stations in frequency and magnitude.

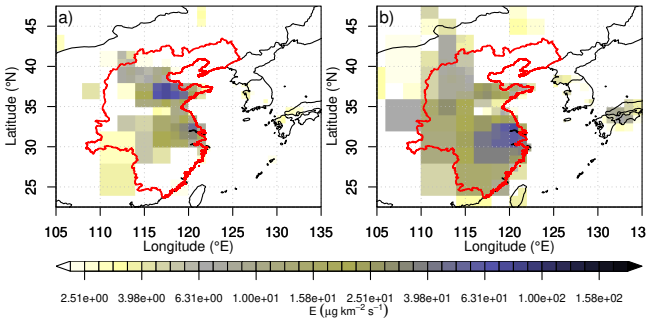

Fig. 4. Posterior HCFC-132b (panel a) and HCFC-133a (panel b) emission distributions (μg km^{-2} s^{-1}) for eastern China based on observations at Gosan (Jeju Island, South Korea) for 2016 – 2019. The red line encloses the area defined as East China.

emissions were greatly reduced. For the period before April 2017, our analysis reveals strong emissions of HCFC-133a near Lyon in south-eastern France, similar to those found earlier using a reduced data set (19), and weaker HCFC-132b emissions close-by. The emissions in this region of intense fluorochemical production ceased after April 2017 and only a secondary potential source of HCFC-133a remains in western Germany. The cessation of measured HCFC-132b and HCFC-133a pollution events in early 2017 could indicate a change in the manufacturing processes in relevant production plants in the area. A possible explanation is the cessation of HFC-134a (CH_2FCF_3) production at Pierre-Bénite (Lyon) in the first quarter of 2017 (33).

Discussion

HCFC-133a and HCFC-31 in the global atmosphere were previously assumed to originate from factory-level emissions during the production of mainly HFC-134a and HFC-143a (CH_3CF_3), and HFC-32 ($CHCl_2F$), respectively (8, 14, 20, 34, 35). HCFC-132b is also likely an intermediate/byproduct involved in reactions to produce HFC-134a and perhaps other HFCs, though we cannot exclude end-use applications. For example, in the widely-used reaction of trichloroethylene ($CHCl{=}CCl_2$) with hydrogen fluoride (HF) to produce HFCs, (foremost HFC-134a), the intermediates CH_2Cl-$CFCl_2$ (HCFC-131a), CH_2Cl-$CClF_2$ (HCFC-132b), and CH_2Cl-CF_3 (HCFC-133a) could potentially be produced and leak to the atmosphere (36). The other isomers of dichlorodifluoroethane are not likely produced from hydrofluorination of HCFC-131a as this would require hydrogen (H) rearrangement, in the case of CHClF-CHClF (HCFC-132) and $CHCl_2$-CHF_2 (HCFC-132a), or nucleophilic substitution of chlorine (Cl) by fluorine (F) on the less favorable carbon atom in the case of CH_2F-CCl_2F (HCFC-132c). This may explain why we did not find these three compounds in the global atmosphere.

Our finding of a strong source of HCFC-133a (and to a lesser extent also of HCFC-132b) in France potentially supports this hypothesis, in particular given the lack of recorded pollution events for both compounds starting with the cessation of the HFC-134a production in that region. On the other hand, for the other (and only remaining) European HFC-134a production site near Frankfurt, HCFC-133a emissions are detected with our method, while those for HCFC-132b are arguably undetectable (Fig. 5, SI).

For the globally dominant emissions, which we locate in East Asia, the predominant source regions for HCFC-132b and HCFC-133a are located in different places. Assuming that both substances are emitted mainly during HFC-134a production, this separation and the large temporal global emission variability, despite monotonically increasing global HFC-134a production, suggest that the generation and leaks of HCFC-132b and HCFC-133a (and HCFC-31 in the case of HFC-32 production) are highly sensitive to industrial practices at the individual HFC production facilities.

Conclusions and Significance

In addition to targeting ODS end-use applications, the Montreal Protocol also addresses feedstock and process emissions, however, with currently no stringent control. The need to place adequate emphasis on these emissions is demonstrated by the example of CCl_4, a compound for which large global unaccounted emissions are found, a large fraction of which are unreported and believed to derive from current industrial production processes (3, 15). We report on emissions of three other ODSs which most-likely fall into this category. Our findings of geographical source separations and large temporal variabilities in the global emissions suggest that some factories temporarily emit much more process-intermediate HCFCs than the low percentages of the end-use compound (HFC) that are commonly assumed (14). These should be identified, and measures applied for emission reductions according to the recommendations of the Montreal Protocol.

While the emissions of these three HCFCs are quantifiable and have increased over the last decades, their ODP-weighted impacts are small compared to those of the major ODSs.

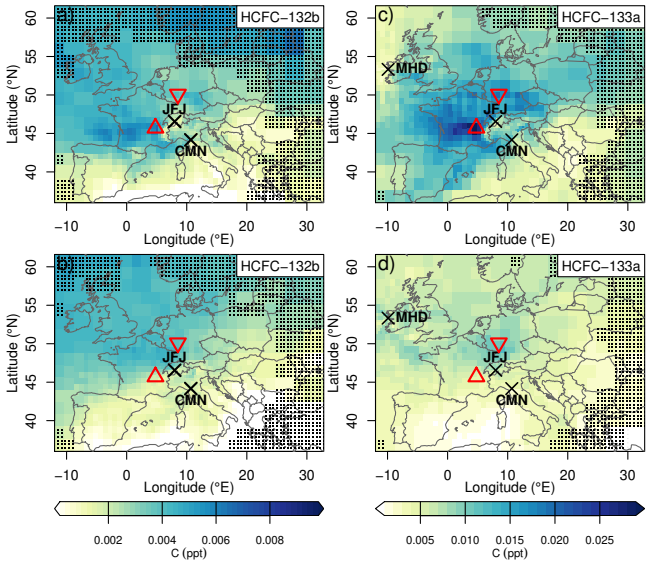

Fig. 5. Potential source areas for European emissions of HCFC-132b and HCFC-133a as estimated by footprint statistics (see supplement). Units refer to average mole fraction enhancements at the receptor sites when influenced by a given grid cell. The upper panels (a and c) are for 2014 – March 2017 and the lower panels (b and d) for April 2017 – 2019. This temporal distinction is made based on the lack of significant pollution events after March 2017. Stations are Mace Head (MHD, Ireland), Jungfraujoch (JFJ, Switzerland), and CMN (Monte Cimone, Italy). Triangles denote HFC-134a factories in France (upward triangle) and Germany (downward triangle). Dotted areas have low source sensitivities and should not be interpreted.

Nevertheless, our findings demonstrate a method for early-warning detection and quantification of nascent emissions of synthetic trace gases based on atmospheric observations. This can, in turn, help to validate inventory-based emissions estimates, uncover potential unreported sources, and enable the assessment of the effectiveness of subsequent mitigation efforts. From an economic perspective, early discovery also enables processes to be changed to reduce unwanted emissions before the scale of the problem becomes more costly to mitigate, as has unfortunately been the case for unaccounted emissions of other compounds (1–7).

More broadly, this study demonstrates the analytical power of modern atmospheric monitoring instrumentation to detect nascent industrial emissions in the atmosphere at sub-ppt levels. It also demonstrates the importance of large-scale global atmospheric network observations and modeling for identifying and quantifying regional emissions. As industrialization continues to expand and move into new regions, the absence of broader regional coverage for such atmospheric observations inhibits a full reconciliation between emissions measured in the global atmosphere and the sum of those determined regionally. The expansion of observational networks will be needed to close such gaps in support of the protection of the stratospheric ozone layer and the climate.

Materials and Methods

Site Description. The AGAGE global network consists of nine fully intercalibrated field stations with long-term measurement records of a suite of ozone depleting substances (ODSs) (27). The network is complemented by affiliated stations and by laboratory instruments, which also serve as urban stations. European field stations are Zeppelin (Spitsbergen), Mace Head (Ireland), Jungfraujoch (Swiss Alps), and the affiliated station Monte Cimone (Italy). Asian stations are located at Gosan (Jeju Island, South Korea) and Shangdianzi (China), however, data from the latter could not be used for this study. Other stations are Trinidad Head (California, USA), Ragged Point (Barbados), Cape Matatula (American Samoa), and Cape Grim (Tasmania, Australia). Measurement records for HCFC-132b and HCFC-133a are of various lengths, with the longest at Jungfraujoch, starting in 2013. In addition to the in situ measurements, flask samples contribute to the analysis presented here. Canister samples are collected weekly at the South Korean Antarctic Station King Sejong (King George Island, South Shetland Islands) (37). Archived air samples used in our analysis derive from the Cape Grim Air Archive (CGAA), which is a set of >120 samples collected since 1978 at the Cape Grim Baseline Air Pollution Station (38–41). Additional archived air samples were collected under clean air conditions in the Northern Hemisphere, mostly at Trinidad Head, La Jolla (California), Boulder (Colorado), and in the Swiss Alps (42).

Data availability: In situ measurements of HCFC-132b and HCFC-133a from the AGAGE stations are available through the AGAGE website at https://agage.mit.edu/. Measurements of the samples collected in flasks, such as for archived air, Antarctica and Dübendorf (HCFC-31), and model results are accessible through https://zenodo.org/, doi: 10.5281/zenodo.4266458.

Measurement Methods. All measurements presented here were conducted using "Medusa" pre-concentration gas chromatography mass spectrometry (GC-MS) instrumentation used in AGAGE (27, 43, 44). HCFC-132b was identified along with the other three isomers of dichlorodifluoroethane to conclusively demonstrate the absence of interferences. Also, with first weekly atmospheric measurements of these three additional isomers starting in mid-2019, and detection levels of ∼0.005 ppt, we find these compounds undetectable within the airmass footprint of the urban station Dübendorf (Switzerland). Due to their atmospheric lifetimes >1 yr (17) we conclude that these three isomers are currently also undetectable in the global atmosphere.

Analytical details for HCFC-133a and HCFC-31 are given in earlier studies (19, 20). Since then, HCFC-133a measurements have been fully integrated into the AGAGE network from which global high-resolution data are now available. Analysis of HCFC-31 is hampered by a coelution with CFC-12 on aged Porabond Q columns (used in AGAGE) and has therefore not been integrated into the network. The HCFC-31 flask sample measurements used in this study were made on the Empa laboratory Medusa-GCMS in a batch mode using a column on which the two compounds could be fully separated, and on a GasPro column on the CSIRO laboratory Medusa (Medusa-9) for the CGAA samples.

Calibration. The present work prompted the development of the Swiss Federal Office of Metrology (METAS) METAS-2017 primary calibration scale for HCFC-132b (45). It is based on 11 dynamically-gravimetrically prepared, Système-International-(SI)-traceable primary reference standards ranging 0.9–1.5 ppt. The calibration scale was adopted into the AGAGE-based Scripps Institution of Oceanography R1 calibration measurement data base and allowed for a reporting of fully intercalibrated measurements used here. The estimated accuracy of this calibration scale is 1.6% (2 σ). Measurements of HCFC-133a are also fully intercalibrated and are based on the Empa-2013 primary calibration scale with an estimated accuracy of 10% (2 σ) (19). For HCFC-132b and HCFC-133a, the calibration scales are propagated from the SIO pool of secondary standards through tertiary traveling standards to on-site quaternary (working) standard. For HCFC-31 the Empa and CSIRO laboratory measurements were intercalibrated and results are based on the Empa-2013 primary calibration scale (20).

Global Emissions derived from Global Chemical Transport Model and Inverse Methods. To derive global emissions that are based on baseline atmospheric observations ("top-down") we employ the AGAGE 12-box model (46–50). The model divides the atmosphere into four zonal bands, separated at the Equator and at the 30° latitudes, thereby creating boxes of similar air masses. The vertical

box separations are at 500 and 200 hPa. We include temperature-dependent hydroxyl (OH) radical reactions, which are the main removal mechanism of all three compounds from the atmosphere (51). We assume stratospheric lifetimes of 45 yr for HCFC-132b, 103 yr for HCFC-133a, and 35 yr for HCFC-31 (26) leading to overall atmospheric lifetimes of 3.4 yr for HCFC-132b, 4.5 yr for HCFC-133a, and 1.4 yr for HCFC-31 in the box model.

Emissions were inferred by comparing model simulations to baseline observations using a Bayesian inverse method in which the emissions growth rate was weakly constrained a priori (29). High frequency observations were filtered to remove "pollution events" using a statistical filter (28), and, combined with archived air samples, averaged into semi-hemispheres. The uncertainty on the observations combined two terms, one related to the measurement repeatability, and one related to the ability of the model to represent the data. The latter was assumed to be equal to the baseline variability for high-frequency samples (or, for flask samples, the average high-frequency variability in the same hemisphere, scaled by mole fraction difference between the flask and high-frequency observations). Some seasonality in emissions was imposed by fitting a sine curve to the emissions, which minimized the model-data mismatch (19). Given the lack of available prior emissions estimates, the annual emissions growth rate was assumed to be zero a priori, with an uncertainty assumed to be 0.1, 1 and 0.1 Gg yr^{-2} for HCFC-132b, HCFC-133a, and HCFC-31, respectively. The derived emissions were found to not strongly depend on these values. The uncertainties in the a posteriori emissions estimates combined uncertainties related to the measurements, model representation error, prior constraint, atmospheric lifetime and calibration scale uncertainty (29). The uncertainty in the lifetime was assumed to be 20% for HCFC-31 (20). For HCFC-133a and HCFC-132b, we assumed lifetime uncertainties equal to the uncertainty in the rate constant with respect to reaction with the hydroxyl radical (10% for HCFC-133a and 50% for HCFC-132b (51)), which we assume to be the largest term in the lifetime uncertainty budget for these substances.

Regional Emission Estimates. The inversion system used to estimate East Asian regional emissions has been previously documented (5, 30). It is here applied to HCFC-132b and HCFC-133a for 2016 – 2019 and using observations from Gosan alone for which pollution events were identified and quantified by subtracting a smooth statistical baseline fit from the observations (52). Source sensitivities were computed with the Lagrangian particle dispersion model FLEXPART version 9.2-Empa driven by operational analysis and forecasts from the European Centre for Medium-Range Weather Forecasts (ECMWF) Integrated Forecasting System employing a horizontal resolution of $0.2^\circ \times 0.2^\circ$ in the area of interest. The Bayesian inversion for East Asia was carried out using a flat a priori emission distribution over all land areas, reflecting our expectation that the emissions are not end-user related and, hence, don't follow population densities. A priori and data-mismatch covariance matrices were constructed using a maximum likelihood approach (30). For European HCFC emissions, the inversion system showed very little skill in reproducing the observed peak concentrations, and is consistent with emissions originating from intermittent sources. Therefore, we applied a more qualitative method to identify potential source areas, which can be seen as a spatially distributed, weighted averaging of the observed concentration increments and builds on a method termed "trajectory statistics" (53) (see SI).

ACKNOWLEDGMENTS. We acknowledge the station personnel at all stations for their continuous support in conducting in situ measurement. Support is also acknowledged for canister sampling at Cape Grim (CSIRO and Bureau of Meteorology), King Sejong (KOPRI), SIO, and for the Dübendorf HCFC-31 record (numerous helpers). We thank Archie McCulloch for valuable discussions on the industrial synthesis of HFC-134a, and possible by-products. The joint Cape Grim Air Archive (CGAA) project is operated by CSIRO and the Australian Bureau of Meteorology. AGAGE operations at Mace Head, Trinidad Head, Cape Matatula, Ragged Point, and Cape Grim are supported by the National Aeronautic and Space Administration (NASA) with grants NAG5-12669, NNX07AE89G, NNX11AF17G, and NNX16AC98G to MIT, grants NNX07AE87G, NNX07AF09G, NNX11AF15G, and NNX11AF16G to SIO, through the Department for Business, Energy & Industrial Strategy (BEIS) contract 1028/06/2015 to the University of Bristol for Mace Head and Tacolneston; the National Oceanic and Atmospheric Administration (NOAA, USA), contracts RA-133-R15-CN-0008 and 1305M319CNRMJ0028 to the University of Bristol for Barbados, by the Commonwealth Scientific and Industrial Research Organization (CSIRO Australia), the Bureau of Meteorology (Australia), the Department of Environment and Energy (Australia) and Refrigerant Reclaim Australia. Financial support for the measurements at the other stations is provided; for Jungfraujoch by the Swiss National Programs HALCLIM and CLIMGAS-CH (Swiss Federal Office for the Environment, FOEN) and by the International Foundation High Altitude Research Stations Jungfraujoch and Gornergrat (HFSJG); for Zeppelin by the Norwegian Environment Agency; for Monte Cimone by the National Research Council of Italy and the Italian Ministry of Education, University and Research through the Project of National Interest Nextdata; for Gosan by the Kyungpook National University Research Fund, 2018. Support for King Sejong flask samples comes from the Swiss State Secretariat for Education and Research and Innovation (SERI) and from the National Research Foundation of Korea for the Korean-Swiss Science and Technology Cooperation Program; and from the Korean Polar Research Programs PE13410 and PE20150. MKV acknowledges support from FOEN and 2016 grants from Empa and the Swiss National Science Foundation (SNSF) for technical development and archived air and firn air measurements at CSIRO Aspendale.

1. Weiss RF, Prinn RG (2011) Quantifying greenhouse-gas emissions from atmospheric measurements: A critical reality check for climate legislation. Philos. Trans. R. Soc. London, Ser. A 369:1925–1942.
2. Arnold T, et al. (2013) Nitrogen trifluoride global emissions estimated from updated atmospheric measurements. Proc. Natl. Acad. Sci. USA 110(6):2029–2034.
3. SPARC (2016) SPARC Report on the Mystery of Carbon Tetrachloride, Technical Report 7, WCRP-13/2016.
4. Montzka SA, et al. (2018) An unexpected and persistent increase in global emissions of ozone-depleting CFC-11. Nature 557:413–417.
5. Rigby M, et al. (2019) Increase in CFC-11 emissions from eastern China based on atmospheric observations. Nature 569:546–550.
6. Simmonds PG, et al. (2020) The increasing atmospheric burden of the greenhouse gas sulfur hexafluoride (SF_6). Atmos. Chem. Phys. 20(12):7271–7290.
7. Stanley KM, et al. (2020) Increase in global emissions of HFC-23 despite near-total expected reductions. Nat Commun 11(397).
8. Laube JC, et al. (2014) Newly detected ozone-depleting substances in the atmosphere. Nat Geosci 7:266–269.
9. Adcock KE, et al. (2018) Continued increase of CFC-113a (CCl_3CF_3) mixing ratios in the global atmosphere: emissions, occurrence and potential sources. Atmos. Chem. Phys. 18(7):4737–4751.
10. Vollmer MK, et al. (2018) Atmospheric histories and emissions of chlorofluorocarbons CFC-13 ($CClF_3$), ΣCFC-114 ($C_2Cl_2F_4$), and CFC-115 (C_2ClF_5). Atmos. Chem. Phys. 18(2):979–1002.
11. Solomon S, Alcamo J, Ravishankara AR (2020) Unfinished business after five decades of ozone-layer science and policy. Nat Commun 11(4272).
12. Lickley M, et al. (2020) Quantifying contributions of chlorofluorocarbon banks to emissions and impacts on the ozone layer and climate. Nat Commun 11(1380).
13. United Nations Environment Programme (2017) Handbook for the Montreal Protocol on Substances that Deplete the Ozone Layer, (United Nations Environment Programme, P.O. Box 30552, Nairobi, Kenya), Technical report.
14. Miller M, Batchelor T (2012) Information paper on feedstock uses of ozone-depleting substances, (Touchdown Consulting), Technical Report European Commission Service Contract No. 07.1201/2011/601842/SER/CLIMA.C2.
15. Sherry D, McCulloch A, Liang Q, Reimann S, Newman PA (2018) Current sources of carbon tertachloride (CCl_4) in our atmosphere. Environ. Res. Lett. 13:024004.
16. United Nations (2016) Montreal Protocol on Substances That Deplete the Ozone Layer. montreal, 16 september 1987. Amendment to the Montreal Protocol on Substances That Deplete the Ozone Layer, kigali, 15 october 2016, (United Nations, New York, 10017), Technical Report C.N.872.2016.TREATIES-XXVII.2.f (Depositary Notification).
17. Papanastasiou DK, Beltrone A, Marshall P, Burkholder JB (2018) Global warming potential estimates for the C_1–C_3 hydrochlorofluorocarbons (HCFCs) included in the Kigali Amendment to the Montreal Protocol. Atmos. Chem. Phys. 18(9):6317–6330.
18. Engel A, et al. (2018) Update on Ozone-Depleting Substances (ODSs) and Other Gases of Interest to the Montreal Protocol, Chapter 1 in Scientific Assessment of Ozone Depletion: 2018, Global Ozone Research and Monitoring Project — Report No. 58. (World Meteorological Organisation, Geneva).
19. Vollmer MK, et al. (2015) Abrupt reversal in emissions and atmospheric abundance of HCFC-133a (CF_3CH_2Cl). Geophys. Res. Lett. 42:8702–8710.
20. Schoenenberger F, et al. (2015) First observations, trends, and emissions of HCFC-31 (CH_2ClF) in the global atmosphere. Geophys. Res. Lett. 42:7817–7824.
21. Pool R (1988) The elusive replacements for CFCs. Science 242(4879):666–668.
22. ECETOC (1990) 1,2-Dichloro-1,1-difluoroethane (HFA-133b) CAS:1649-08-7, (European

Chemical Industry Ecology and Toxicology Centre, Brussels), Technical Report JAAC 011.
23. ECETOC (1990) 1-Chloro-2,2,2-trifluoroethane (HFA-133a) CAS:75-88-7, (European Chemical Industry Ecology and Toxicology Centre, Brussels), Technical Report JAAC 014.
24. Anders MW (1991) Metabolism and toxicity of hydrochlorofluorocarbons: Current knowledge and needs for the future. Environ. Health Perspect. 96:185–191.
25. DFG (Deutsche Forschungsgemeinschaft) (2018) List of MAK and BAT Values 2018: Maximum Concentrations and Biological Tolerance Values at the Workplace, Permanent Senate Commission for the Investigation of Health Hazards of Chemical Compounds in the Work Area. (WILEY-VCH Verlag GmbH & Co. KGaA, Weinheim) No. 54, p. 642.
26. Burkholder J, Hodnebrog Ø, Orkin VL (2018) Summary of Abundances, Lifetimes, Ozone Depletion Potentials (ODPs), Radiative Efficiencies (REs), Global Warming Potentials (GWPs), and Global Temperature change Potentials (GTPs), Appendix A in Scientific Assessment of Ozone Depletion: 2018, Global Ozone Research and Monitoring Project — Report No. 58. (World Meteorological Organisation, Geneva).
27. Prinn RG, et al. (2018) History of chemically and radiatively important atmospheric gases from the Advanced Global Atmospheric Gases Experiment (AGAGE). Earth Syst. Sci. Data 10(2):985–1018.
28. O'Doherty S, et al. (2001) In situ chloroform measurements at Advanced Global Atmospheric Gases Experiment atmospheric research stations from 1994 to 1998. J. Geophys. Res. 106(D17):20429–20444.
29. Rigby M, et al. (2014) Recent and future trends in synthetic greenhouse gas radiative forcing. Geophys. Res. Lett. 41:2623–2630.
30. Henne S, et al. (2016) Validation of the Swiss methane emission inventory by atmospheric observations and inverse modelling. Atmos. Chem. Phys. 16(6):3683–3710.
31. Fang X, et al. (2019) Rapid increase of ozone-depleting chloroform emissions from China. Nat Geosci 12:89–93.
32. Lunt MF, et al. (2018) Continued emissions of the ozone-depleting substance carbon tetrachloride from Eastern Asia. Geophys. Res. Lett. 45(20):11423–11430.
33. Arkema (2016) Proposed closure of the R134a fluorogas activity on the Pierre-Bénite site. https://www.arkema.com/en/media/news/news-details/Proposed-closure-of-the-R134a-fluorogas-activity-on-the-Pierre-Benite-site/, last accessed 12 November 2019.
34. Shanthan Rao P, Narsaiah B, Rambabu Y, Sridhar M, V. RK (2015) Catalytic processes for fluorochemicals: Sustainable alternatives in Industrial Catalysis and Separations: Innovations for Process Intensification, eds. Raghavan KV, Reddy BM. (Apple Academic Press, Toronto), pp. 407–435.
35. Vollmer MK, Reimann S, Hill M, Brunner D (2015) First observations of the fourth generation synthetic halocarbons HFC-1234yf, HFC-1234ze(E), and HCFC-1233zd(E) in the atmosphere. Environ. Sci. Technol. 49:2703–2708.
36. Belter RK, Bhamare NK (2006) Solvent effects in the fluorination of 1,2-dichloro-1,1-difluoroethane (R-132b) to 2-chloro-1,1,1-trifluoroethane (R-133a). J. Fluorine Chem. 127:1606–1610.
37. Vollmer MK, et al. (2011) Atmospheric histories and global emissions of the anthropogenic hydrofluorocarbons HFC-365mfc, HFC-245fa, HFC-227ea, and HFC-236fa. J. Geophys. Res. 116:D08304.
38. Fraser PJ, Langenfelds R, Derek N, Porter LW (1991) Studies in air archiving techniques. part 1: Long term stability of atmospheric trace gases in dry, natural air stored in high-pressure, surface-treated aluminium cylinders in Baseline Atmospheric Program Australia 1989, eds. Wilson SR, Gras JL. (Bureau of Meteorology and CSIRO Division of Atmospheric Research, Canberra, Australia) Vol. 1989, pp. 16–29.
39. Langenfelds RL, et al. (1996) The Cape Grim air archive: The first seventeen years, 1978–1995 in Baseline Atmospheric Program (Australia) 1994-95, eds. Francey RJ, Dick AL, Derek N. (Bureau of Meteorology and CSIRO Division of Atmospheric Research, Australian Bureau of Meteorology and CSIRO Marine and Atmospheric Research, Melbourne, Australia), pp. 53–70.
40. Langenfelds RL, et al. (2014) Archiving of Cape Grim air in Baseline Atmospheric Program Australia 2009-2010, eds. Derek N, Krummel PB, Cleland SJ. (Australian Bureau of Meteorology and CSIRO Marine and Atmospheric Research, Melbourne, Australia), pp. 44–45.
41. Fraser PJ, et al. (2016) Non-carbon dioxide greenhouse gases at Cape Grim: a 40 year odyssey in Baseline Atmospheric Program (Australia) History and Recollections, 40th Anniversary Special Edition, eds. Derek N, Krummel PB, Cleland SJ. (Bureau of Meteorology and CSIRO Oceans and Atmosphere, Melbourne, Australia), pp. 45–76.
42. Vollmer MK, et al. (2015) Modern inhalation anesthetics: Potent greenhouse gases in the global atmosphere. Geophys. Res. Lett. 42:1606–1611.
43. Miller BR, et al. (2008) Medusa: A sample preconcentration and GC/MS detector system for in situ measurements of atmospheric trace halocarbons, hydrocarbons, and sulfur compounds. Anal. Chem. 80(5):1536–1545.
44. Arnold T, et al. (2012) Automated measurement of nitrogen trifluoride in ambient air. Anal. Chem. 84:4798–4804.
45. Guillevic M, et al. (2018) Dynamic–gravimetric preparation of metrologically traceable primary calibration standards for halogenated greenhouse gases. Atmos. Meas. Tech. 11(6):3351–3372.
46. Cunnold DM, et al. (1983) The atmospheric lifetime experiment 3. Lifetime methodology and application to 3 years of $CFCl_3$ data. J. Geophys. Res. 88(NC13):8379–8400.
47. Cunnold DM, et al. (1994) Global trends and annual releases of CCl_3F and CCl_2F_2 estimated from ALE/GAGE and other measurements from July 1978 to June 1991. J. Geophys. Res. 99(D1):1107–1126.
48. Cunnold DM, et al. (1997) GAGE/AGAGE measurements indicating reductions in global emissions of CCl_3F and CCl_2F in 1992-1994. J. Geophys. Res. 102(D1):1259–1269.
49. Rigby M, et al. (2013) Re-evaluation of lifetimes of the major CFCs and CH_3CCl_3 using atmospheric trends. Atmos. Chem. Phys. 13:2691–2702.
50. Vollmer MK, et al. (2016) Atmospheric histories and global emissions of halons H-1211 ($CBrClF_2$), H-1301 ($CBrF_3$), and H-2402 ($CBrF_2CBrF_2$). J. Geophys. Res. Atmos. 121:3663–3686.
51. Burkholder JB, et al. (2015) Chemical kinetics and photochemical data for use in atmospheric studies, evaluation no. 18 of the NASA panel for data evaluation, (Jet Propulsion Laboratory, Pasadena), JPL Publication 15-10.
52. Ruckstuhl AF, et al. (2012) Robust extraction of baseline signal of atmospheric trace species using local regression. Atmos. Meas. Tech. 5:2613–2624.
53. Stohl A (1996) Trajectory statistics - a new method to establish source-receptor relationships of air pollutants and its application to the transport of particulate sulfate in Europe. Atmos. Environ. 30(4):579–587.

Supporting Information Text

Analytical Details. For the present work, GCMS identification of HCFC-132b (1,2-dichloro-1,1-difluoroethane) was conducted on the Medusa-GCMS instruments based on a diluted sample from the pure compound obtained commercially (SynQuest Laboratories, Alachua, Florida, USA). The compound was characterized by chromatographic retention time and mass spectrum on the Empa laboratory Medusa-GCMS (serial number Medusa-20, Tables S1 and S2). In addition to HCFC-132b, there are three more isomers of dichlorodifluoroethane, which were also characterized to check for potential interference with HCFC-132b. Again, for these, the pure substances were obtained (SynQuest Laboratories) and identified on the GCMS based on a diluted sample. These three other isomers of dichlorodifluoroethane are HCFC-132 (1,2-dichloro-1,2-difluoroethane), HCFC-132a (1,1-dichloro-2,2-difluoroethane), and HCFC-132c (1,1-dichloro-1,2-difluoroethane). Based on these findings we conclude that our measurements of HCFC-132b are not interfering with any of the other isomers. The Empa Medusa-20 GCMS is fitted with the AGAGE-wide used Porabond Q chromatography column (1). Retention times on this column are given in Table S1 with marker halocarbon substances eluting nearby.

Mass spectra of the four isomers were measured using the Empa Medusa-20 GCMS (Table S2). Those for HCFC-132a and HCFC-132b could be compared to the spectra available from the National Institute of Standards and Technology (NIST) (https://webbook.nist.gov/chemistry/, last accessed 27 June 2019) and showed good agreement to our results. The mass spectra for HCFC-132 and HCFC-132c listed here in Table S2 are to the best of our knowledge the first publicly available. The mass/charge (m/z) 44 (likely the fragment C_2HF^+) was present in all four spectra but interfered with a CO_2^+ background and was therefore difficult to quantify. The m/z 49 is listed as fragment CH_2Cl^+ in Table S2 but for HCFC-132 and HCFC-132a, this would only be possible with an atom recombination. More details on the GCMS characterization for HCFC-133a and HCFC-31 are given in earlier publications (2, 3).

Table S1. Chemical details and gas chromatography retention times for four isomers of dichlorodifluoroethane, 2-chloro-1,1,1-trifluoroethane (HCFC-133a), and chlorofluoromethane (HCFC-31).

	HCFC-132	HCFC-132a	HCFC-132b	HCFC-132c	HCFC-133a	HCFC-31
Formula	$CHClFCHClF$	$CHCl_2CHF_2$	$CH_2ClCClF_2$	CH_2FCCl_2F	CH_2ClCF_3	CH_2ClF
CAS Registry Number	431-06-1	471-43-2	1649-08-7	1842-05-3	75-88-7	593-70-4
Boiling Point (°C)	58–59	60	46–47	45	6.9	–9
Retention Time Porabond Q (sec)	1447	1446	1420	1416	1313	1221
Nearby eluting Halocarbon[a]	$CHCl_3$ (1451)	H-2402 (1442)	CFC-113 (1432)	CFC-113 (1432)	CFC-114 (1314)	CFC-12 (1230)
Retention Time Gaspro[b] (sec)	1764	1759	1694	1703	1577	1523
Nearby eluting Halocarbon[a, b]	CH_3CCl_3 (1799)	TCE (1738)	CCl_4 (1699)	CCl_4 (1699)	CFC-11 (1563)	CFC-114 (1526)

a) number in parentheses are retention times in seconds
b) For a 60-m Gaspro column fitted into a different instrument

Table S2. Mass spectra for four isomers of dichlorodifluoroethane based on gas-chromatography Electron-Impact (EI) ionization mass spectrometry.[a]

HCFC-132 $CHClFCHClF$ this work			HCFC-132a $CHCl_2CHF_2$ this work				NIST[b]			HCFC-132b $CH_2ClCClF_2$ this work				NIST[b]			HCFC-132c CH_2FCCl_2F this work		
A	M	F	A	M	F		A	M	F	A	M	F		A	M	F	A	M	F
%	m/z		%	m/z			%	m/z		%	m/z			%	m/z		%	m/z	
100	67	$CHClF^+$	100	83	$CHCl_2^+$		100	83	$CHCl_2^+$	100	99	$C_2H_2ClF_2^+$		100	99	$C_2H_2ClF_2^+$	100	99	$C_2H_2ClF_2^+$
67	99	$C_2H_2ClF_2^+$	65	85	$CH^{35}Cl^{37}Cl^+$		67	85	$CH^{35}Cl^{37}Cl^+$	32	101	$C_2H_2{}^{37}ClF_2^+$		32	49	CH_2Cl^+	89	101	$C_2H_2{}^{37}ClF_2^+$
33	69	$CH^{37}ClF^+$	34	134	$C_2H_2Cl_2F_2^+$		24	134	$C_2H_2Cl_2F_2^+$	16	85	$CClF_2^+$		29	101	$C_2H_2{}^{37}ClF_2^+$			CCl_2F^+
31	79	C_2HClF^+	20	136	$C_2H_2{}^{35}Cl^{37}ClF_2^+$		15	136	$C_2H_2{}^{35}Cl^{37}ClF_2^+$	14	79	C_2HClF^+		20	85	$CClF_2^+$	37	103	$C^{35}Cl^{37}ClF^+$
22	101	$C_2H_2{}^{37}ClF_2^+$	16	51	CHF_2^+		12	51	CHF_2^+	13	49	CH_2Cl^+		15	79	C_2HClF^+	24	79	C_2HClF^+
14	134	$C_2H_2Cl_2F_2^+$	14	99	$C_2H_2ClF_2^+$		11	87	$CH^{37}Cl_2^+$	5	87	$C^{37}ClF_2^+$		11	51	$CH_2{}^{37}Cl$	8	81	$C_2H^{37}ClF^+$
10	81	$C_2H^{37}ClF^+$	14	79	C_2HClF^+		10	49	CH_2Cl^+	5	51	$CH_2{}^{37}Cl$		7	87	$C^{37}ClF_2^+$	7	49	CH_2Cl^+
9	136	$C_2H_2{}^{35}Cl^{37}ClF_2^+$	11	87	$CH^{37}Cl_2^+$		9	133	$C_2HCl_2F_2^+$	5	64	$C_2H_2F_2^+$		7	64	$C_2H_2F_2^+$	7	105	$C^{37}Cl_2F^+$
8	49	CH_2Cl^+	9	49	CH_2Cl^+		9	99	$C_2H_2ClF_2^+$	5	81	$C_2H^{37}ClF^+$		7	31	CF^+	4	64	$C_2H_2F_2^+$
							8	79	C_2HClF^+					7	81	$C_2H^{37}ClF^+$	4	63	$C_2HF_2^+$

a) These measurements were carried out using a Medusa-GCMS (Agilent Technologies GC 6890 and a quadrupole MS 5975) located in the Empa laboratory (Medusa-20). Mass/Charge (m/z) acquisition range was chosen 40–250. Abbreviations are: A: Abundance of fragment, relative to most abundant fragment (in %). M: m/z of measured fragment. F: Assumed main fragment(s) for this m/z.
b) Spectra from the National Institute of Standards and Technology (NIST) were taken from https://webbook.nist.gov/chemistry/, last accessed 27 June 2019.

Full Historic Records. For a clearer description of the more recent record, only a limited time-range for the global record is given in the main text. Here we show the full historic record dating back to 1978 (Fig. S1). For HCFC-31 samples measured on the Medusa GCMS located at CSIRO (aspendale-medusa), which are mainly those of the Cape Grim Air Archive (CGAA), detection limits were relatively poor (25 ppq, parts-per-quadrillion, femtomol mol^{-1}). Reanalysis of some CGAA subsamples back to 1998 on an instrument at Empa (empa-medusa), with significantly lower detection limits, revealed HCFC-31 mole fractions of ∼18 ppq for the period 1998–2004. Because such highly sensitive measurements are lacking for samples older than 1998, their HCFC-31 mole fractions can only be approximated with the poorer detection limits, i.e. <25 ppq. This is indicated by the grey shaded area in Fig. S1.

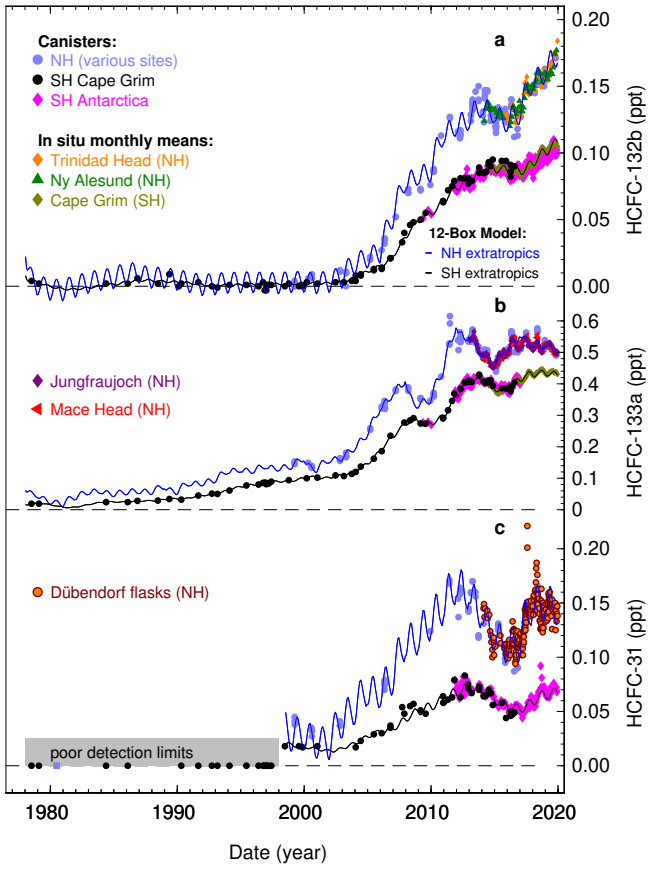

Fig. S1. Full (1978 – present) record of atmospheric observations and model reconstructions of the hydrochlorofluorocarbons (HCFCs) HCFC-132b, HCFC-133a, and HCFC-31. For clarity, flask sample results for HCFC-132b and HCFC-133a from various Northern Hemisphere sites are aggregated into a single data set. Flask samples for the Southern Hemisphere are shown for Cape Grim (Tasmania) and the Antarctic station King Sejong. In-situ records for HCFC-132b and HCFC-133a from stations of the Advanced Global Atmospheric Gases Experiment (AGAGE) are shown here as background-filtered monthly means for a few exemplary stations. Modeled records derive from the observations and an inversion system using a 12-box chemical transport model, and are shown for the four ground-level model boxes. Results for HCFC-133a and HCFC-31 are significant updates to earlier studies (2, 3). For HCFC-132b measurements in the Cape Grim Air Archive (CGAA), a chromatographic memory correction was necessary, which caused some of the near-zero mole fractions to become negative.

Other Source Regions. Our analysis shows that for HCFC-132b, East Asian emissions can largely explain the global emissions. However, for HCFC-133a we attribute only ∼80% of global emissions to East Asia, thus raising the question of the origin of the remaining fraction of ∼20%. Apart from East Asian and European source regions, the current AGAGE network is sensitive only to a few regions in the world. Emissions from Europe are detected, but these are not significant. For North America, measurements at the Trinidad Head AGAGE station in northern California are sensitive only to emissions from parts of the coastal western US (4). During its 4-year record for HCFC-132b and HCFC-133a, only a few minor enhancements of these compounds were found in air that has passed over the western US, while the majority of such minor enhancements were observed in strong westerly winds originating from Asia. These data are insufficient to draw any conclusions regarding potential North American sources. Significant contamination of these compounds in HFC-134a used in mobile air conditioners is unlikely. If, as we hypothesize, these new compounds are emitted as intermediate products during HFC production, with the majority of US fluorocarbon production facilities located in its eastern states, the AGAGE network would be insensitive to these sources. In Australia, the Cape Grim AGAGE station has significant sensitivity to some densely populated areas in southern Australia, including Melbourne. During its six-year measurement record for HCFC-132b and HCFC-133a, no significant enhancements above background values were observed, so it is unlikely that significant emissions originate from this

region. Given the limited coverage of existing observing stations around the globe, it is currently not possible to draw further conclusions regarding the sources of the remaining ∼20% of global HCFC-133a emissions.

Source Regions for HCFC-31. HCFC-31 could potentially be emitted from similar East Asian regions as HCFC-132b and HCFC-133a. As is suspected in the literature (see ref (3) and references therein), a certain fraction of the observed HCFC-31 in the atmosphere could stem from HFC-32 production. This would therefore imply that HCFC-31 could be emitted from East Asia, as HFC-32 production plants are largely located in that region. Unfortunately, analytical limitations and limited resources within the AGAGE network prevent continuous measurements of HCFC-31 at stations that include East Asia in their footprints. An alternative could be to establish a flask sampling program for this region, with analysis on a laboratory instrument which is setup to measure HCFC-31 (3). However, costs for such program would be large and interpretations from flask samples may be limited, potentially preventing us from reporting more than sporadic samples of elevated HCFC-31.

Possible sources from halocarbon degradation and impurities. We hypothesize that the three HCFCs are emitted as intermediate or byproducts during HFC production. Here we explore halocarbon degradation and HFC impurities as other potential sources: HCFC-31 is a known degradation product of CFC-11 and HCFC-21 under anaerobic conditions, such as in landfills or composts (3). We have not found any direct evidence that point to HCFC-133a or HCFC-132b as degradation products of other halocarbons. Based on similarity arguments of the above-mentioned dechlorination product HCFC-31, and literature findings for HCFC-133 and HCFC-133b as decay products of CFC-113 (5), we speculate that HCFC-133a could result from degradation of CFC-113a and HCFC-123, and HCFC-132b from degradation of CFC-112a and HCFC-122a. However, these educts are found or assumed to be present only at low abundances in the atmosphere (6), hence the resulting quantities of HCFC-133a and HCFC-132b would be insignificant.

We have also investigated the possibility that the three HCFCs are emitted as impurities in commercially used HFCs. First, we investigated ambient air samples elevated with HCFC-133a or HCFC-132b observed at European stations and Gosan station, but found no coincident major enhancements of commercially used HFCs. Second, we inspected other samples with large HFC contamination for HCFC-133a and HFC-132b. Elevated HCFC-133a was found in one case for laboratory air contaminated with HFCs from an air conditioner and in another case in indoor samples from a company dealing with refrigerants. However, for HFC-134a mole fractions of 200 ppb to 1000 ppb (nanomol mol^{-1}), HCFC-133a was only elevated by approx. 0.5 ppt, roughly corresponding to a molar ratio of these compounds of 10^{-6}. Apart from HFC-134a other HFCs (e.g. HFC-125, HFC-143a) were also highly elevated in these samples preventing us from conclusively pointing to a single HFC as potential source for HCFC-133a impurities. Nevertheless such small impurity ratios cannot explain the observed major pollution events in East Asia nor the global emission ratio of HCFC-133a to those of the HFCs (7).

HCFC-31 measurements from urban Dübendorf (Fig. S1c) show a few flask samples with elevated HCFC-31. These were not significantly elevated in HFC-32. In general, elevated HFC-32 in the flask samples did not generally exhibit elevated HCFC-31. We also inspected pure HFC-32 (SynQuest Laboratories Inc, Alachua, Florida, USA) and found small amounts of HCFC-31 with a molar ratio HCFC-31/HFC-32 of 1.7×10^{-6}. This impurity ratio, and also one found for HCFC-133a in HFC-134a (molar ratio 10^{-6}, (2)) are too small to explain the global emissions of these HCFCs when scaled to the global emissions of the HFCs. However these measurements were conducted on research-grade HFC samples (SynQuest Laboratories) and may not be representative of the globally large-scale factory produced HFCs.

European Pollution Events. The European field stations (Zeppelin, Spitsbergen; Mace Head, Ireland; Tacolneston, United Kingdom; Jungfraujoch, Switzerland; Monte Cimone, Italy) revealed a very unusual pattern of regional pollution events for both HCFC-132b and HCFC-133a (Fig. S2). Unlike for other halocarbons, where all but the Zeppelin station usually record frequent and significant pollution events (8), we find very sporadic pollution events for these two compounds. However these are very pronounced and many of them occurred simultaneously for the two compounds at an individual site (e.g. Jungfraujoch). Also, pollution events at Jungfraujoch coincided temporarily with events recorded at Monte Cimone. For HCFC-132b, no pollution events were recorded in the relatively short records at Mace Head (starting November 2017) and Tacolneston (starting January 2019). For HCFC-133a only one pollution event was recorded at Mace Head (record starts in February 2014) but three distinct pollution events were recorded at Tacolneston (record starts in February 2015). No pollution event was detected for either compound at Zeppelin. At the urban station Dübendorf (Zurich, Switzerland) pollution events occurred at about twice the frequency of those at Jungfraujoch, but with many temporarily coinciding. Most remarkably, pollution events for both compounds at all European field stations ceased in early 2017. At urban Dübendorf, HCFC-132b pollution events also ceased at that time while for HCFC-133a a few pollution events were recorded past that date.

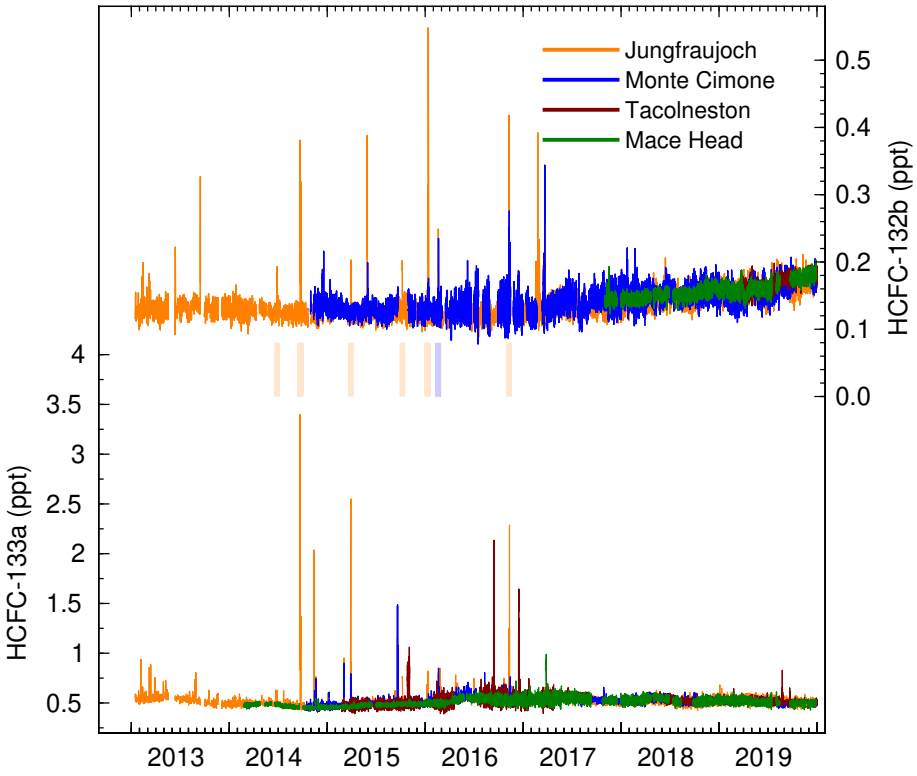

Fig. S2. Atmospheric observations of the hydrochlorofluorocarbons (HCFCs) HCFC-132b and HCFC-133a for the European stations Jungfraujoch, Monte Cimone, Mace Head, and Tacolneston. Pollution events at these three sites are rare, with those at Mace Head limited to a single event. Pollution events show remarkable temporal coincidence between Jungfraujoch and Monte Cimone, and between the two compounds. Vertical light-shaded bars show simultaneous pollution events at Jungfraujoch (light orange) and Monte Cimone (light blue). The lack of observed pollution events after early 2017 is in agreement with the announced closure of the HFC-134a production at Pierre-Bénite (Southeast France) for spring 2017 (9), and our regional footprint statistic pointing to that region as a potential source of emissions for these compounds.

Empa Bayesian Regional Inversion System (EBIRS). For both the East Asian region (with the observations from Gosan) and for Europe (with the observations from Jungfraujoch, Monte Cimone and Mace Head) we applied the regional inverse modelling system EBRIS as described in detail by Henne et al. (10) and previously applied to halocarbon emissions (e.g., 11–13). The inversion system uses source sensitivities as calculated by the Lagrangian Particle Dispersion Model FLEXPART (14). The model was run in time-inverted mode releasing 50,000 model particles within 3-hourly intervals at each observation location and tracing these back for 10 days in the global atmosphere. FLEXPART was driven by operational analysis fields of the Integrated Model System (IFS) of the European Centre for Medium-Range Weather Forecasts (ECMWF) with a horizontal resolution of 0.2° by 0.2° in the target areas (East China, Central Europe) and 1° by 1° elsewhere. The inversion employs the atmospheric observations and the simulated source sensitivities in a Bayesian inference of gridded temporal mean emissions in the target regions. In addition, a temporally resolved baseline mole fraction is statistically derived from the observations (15) and optimised through the inversion. The inversion requires spatially resolved a priori emissions. For all target domains (East Asia and Central Europe) and for all compounds (HCFC-132b and HCFC-133a) a priori emissions were set to a constant value over all land areas: 0.9 g yr^{-1} km^{-2} and 2.6 g yr^{-1} km^{-2} for both compounds and for East Asia and Central Europe, respectively. These values are roughly based on the global GDP share of the specific regions. The flat a priori is reflecting our lack of information on where emissions actually may occur. This is in contrast to compounds with well defined use scenarios, for which either a population-based or emission process-based a priori could be assigned.

For East Asia two sets of sensitivity inversions were run that differed in the applied structure of the a priori and data-mismatch covariance matrices. For the first, a set of parameters describing the covariance were selected by expert judgement and by iteratively evaluating simulation-observation residuals. In the second approach the parameters were estimated by maximum likelihood evaluation for annual inversion batches (10). Differences between the two sensitivity inversions were small and all presented a priori results represent an average over both sensitivity runs. For the European domain only one set set of sensitivity inversions was conducted, which used the same set-up of covariance parameters as the first sensitivity inversion for the East Asian domain. However, the model a posteriori simulations showed very limited skill in predicting the observed pollution peaks. This could be indicative of an intermittent nature of the emission source, which is difficult for the inversion system as it is targeted at annual average emissions. Hence, we do not present the absolute numbers of the derived a posteriori emissions, but rather use the derived spatial distribution to identify potential source areas and their changes over time.

The result of the inversion are spatially resolved a posteriori emission fluxes. We aggregated these within specific regions and countries to discuss the temporal evolution of emissions. For East Asia emissions within the following regions/countries were

summarised: West and East China, Taiwan, Japan, North Korea, and South Korea. East China was defined as the Chinese provinces (north to south): Liaoning, Hebei, Beijing, Tianjin, Shanxi, Shandong, Henan, Anhui, Jiangsu, Hubei, Shanghai, Zhejiang, Jiangxi, and Fujian; whereas all other Chinese provinces were summarised as West China. For regions/countries that were not fully covered by the inversion grid (West China, Japan) the final by-region a posteriori emissions were calculated by using population distributions to scale up the emissions from the covered part of the region to the whole region. This resulted in considerably larger a posteriori uncertainties for such regions compared to fully covered regions. Average a posteriori emissions for the whole inversion domain are shown in Fig. S3, whereas contributions by region are given in Fig. S4.

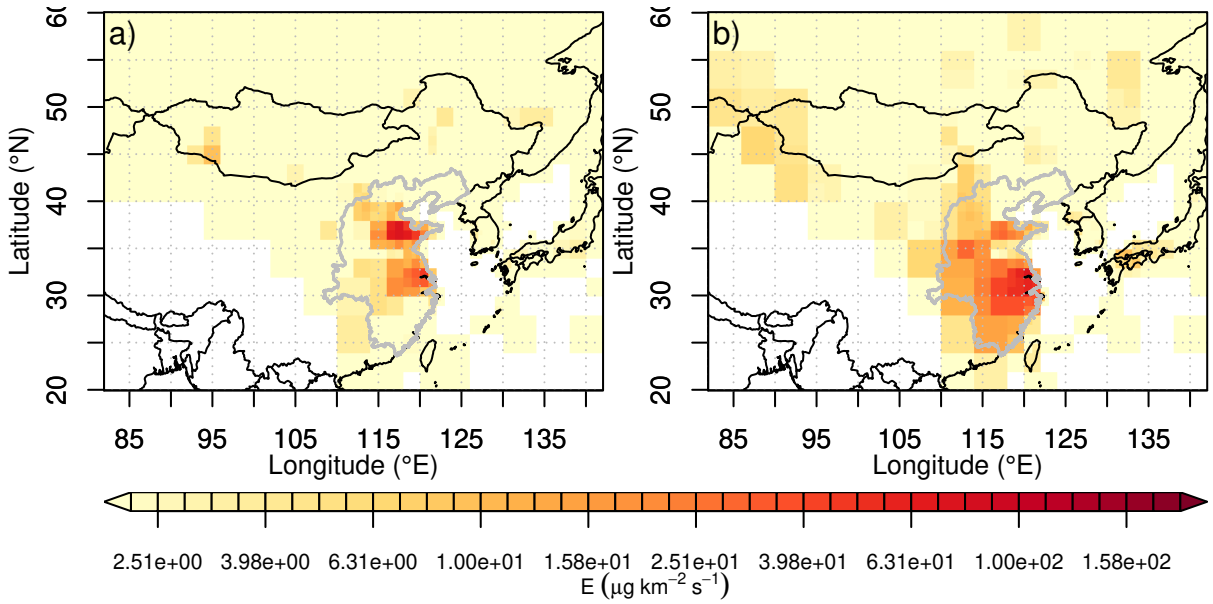

Fig. S3. Posterior HCFC-132b (panel a) and HCFC-133a (panel b) emission distributions (μg km^{-2} s^{-1}) for East Asia based on observations at Gosan (Jeju Island, South Korea) for 2016 – 2019. The gray lines outlines the region defined as East China. White areas are either completely over the ocean or were not sufficiently well covered by the footprint of Gosan and as such omitted from the inversion grid.

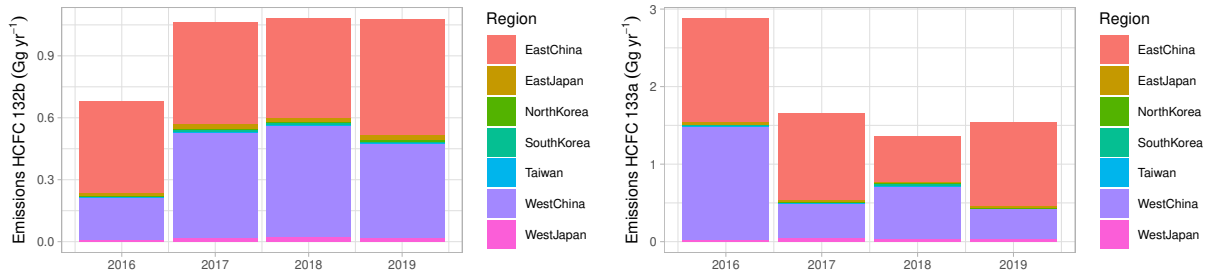

Fig. S4. Posterior HCFC-132b (left) and HCFC-133a (right) emissions per region for East Asian region based on observations at Gosan (Jeju Island, South Korea) for 2016 – 2019.

Potential Source Contributions. In addition to the Bayesian inversion, two alternative statistical, qualitative approaches were taken to identify potential source regions/locations of HCFC-132b and HCFC-133a in Europe. The first (footprint statistics) is based on the method developed by Stohl (16) for individual back-trajectories. Instead of individual trajectories we use the same source sensitivities as were derived for the Bayesian inversion. These and the mole fraction enhancements over the statistical baseline (15) are then used to derive a spatially-resolved, weighted average mole fraction. Areas with larger mole fractions can then be interpreted as potential source areas.

The second method (potential source contribution) follows the approach originally developed by Ashbaugh et al. (17) for back-trajectories. Again we replace individual back-trajectories by source sensitivities and evaluate the average source sensitivity distribution for times when pollution events were recorded (H) against average source sensitivities of all times (T). For this analysis pollution events were defined as times when the HCFC-133a and HCFC-132b mole fraction at a site was 0.05 ppt and 0.03 ppt above the baseline mole fraction, respectively. As a comparison statistic we calculate $(H - T)/T$ and display this in units percent. Once again, large values can then be interpreted as potential source areas.

For both methods, results in areas with generally low source sensitivities, reflecting infrequent and/or weak influence on the observations, are statistically not sound and should not be interpreted.

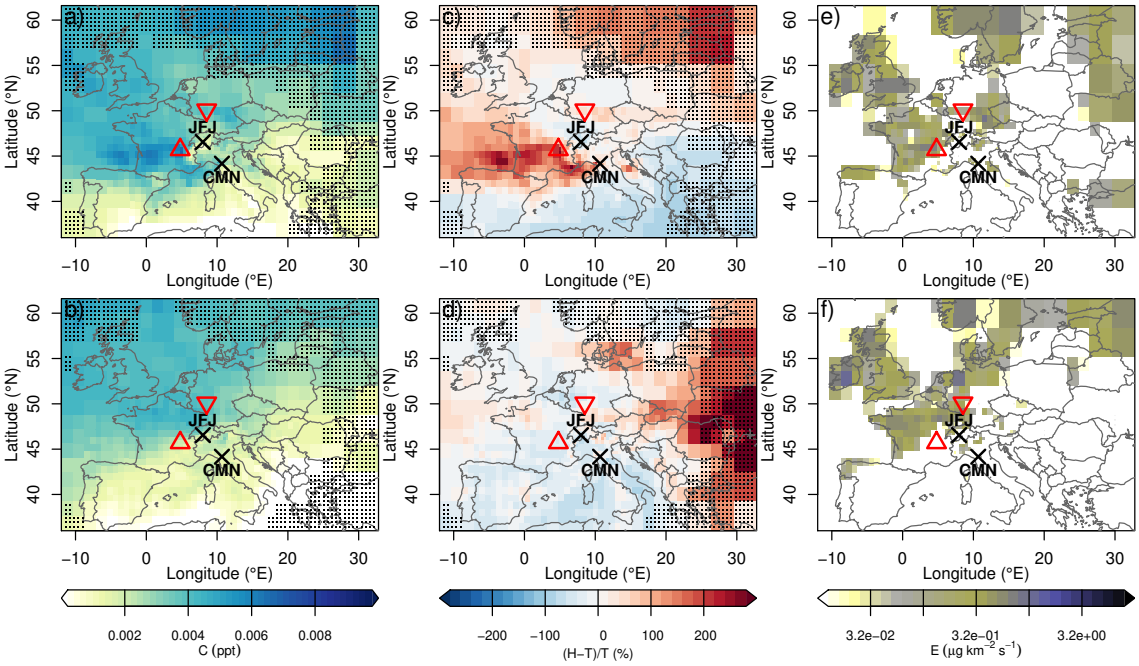

Fig. S5. Potential source areas of HCFC-132b in Europe as indicated by footprint statistics (a, b), potential source contribution (c, d), and a posteriori of Bayesian inversion (e, f). The red triangles denote the two European HFC-134a production plants. Two periods were analysed: before April 2017 (a, c, e) and after April 2017 (b, d, f) when HFC-134a production ceased in South-eastern France (9). Crosses indicate the measurement sites used in this analysis, these are Jungfraujoch (JFJ, Switzerland) and Monte Cimone (CMN, Italy). Dotted areas have low source sensitivities and should not be interpreted.

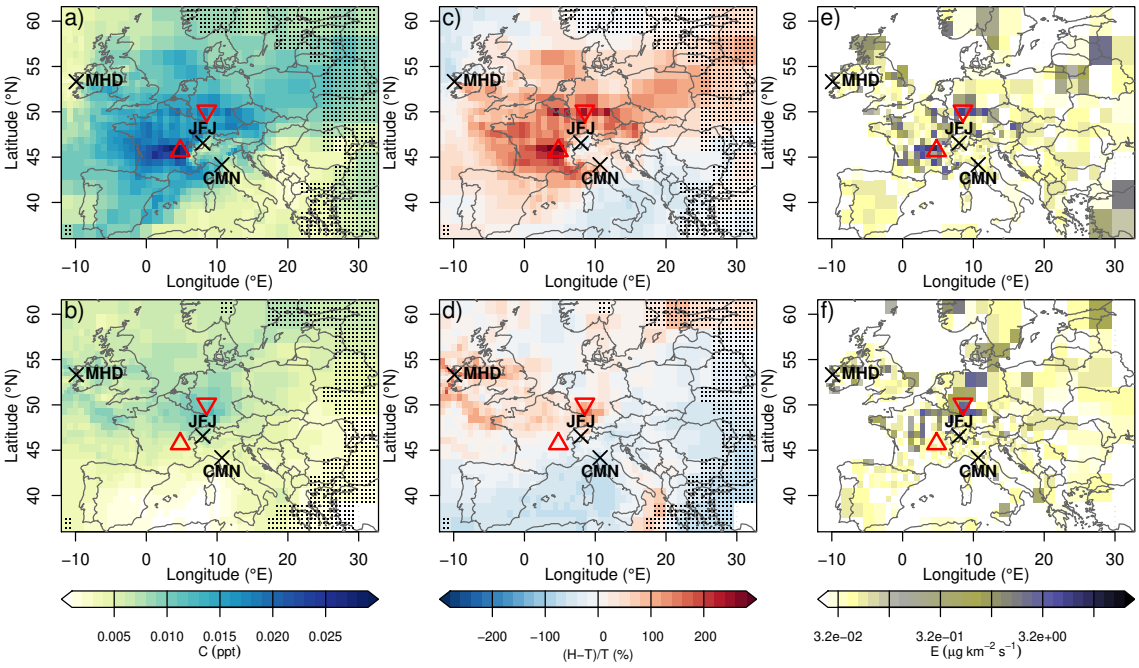

Fig. S6. Potential source areas of HCFC-133a in Europe as indicated by footprint statistics (a, b), potential source contribution (c, d), and a posteriori of Bayesian inversion (e, f). The red triangles denote the two European HFC-134a production plants. Two periods were analysed: before April 2017 (a, c, e) and after April 2017 (b, d, f) when HFC-134a production ceased in South-eastern France (9). Crosses indicate the measurement sites used in this analysis, these are Mace Head (MHD, Ireland), Jungfraujoch (JFJ, Switzerland) and Monte Cimone (CMN, Italy). Dotted areas have low source sensitivities and should not be interpreted.

References

1. Miller BR, et al. (2008) Medusa: A sample preconcentration and GC/MS detector system for in situ measurements of atmospheric trace halocarbons, hydrocarbons, and sulfur compounds. *Anal. Chem.* 80(5):1536–1545.
2. Vollmer MK, et al. (2015) Abrupt reversal in emissions and atmospheric abundance of HCFC-133a (CF_3CH_2Cl). *Geophys. Res. Lett.* 42:8702–8710.
3. Schoenenberger F, et al. (2015) First observations, trends, and emissions of HCFC-31 (CH_2ClF) in the global atmosphere. *Geophys. Res. Lett.* 42:7817–7824.
4. Manning AJ, et al. (2008) Quantifying regional greenhouse gas emissions of HFC-134a from atmospheric measurements at the Trinidad Head (California), Cape Grim (Tasmania) and Mace Head (Ireland) remote AGAGE sites. *Eos Trans. AGU.* AGU 2008 Fall Meeting Suppl., Abstract A53H-01.
5. Lesage S, Brown S, Hosler KR (1992) Degradation of chlorofluorocarbon-113 under anaerobic conditions. *Chemosphere* 24(9):1225–1243.
6. Laube JC, et al. (2014) Newly detected ozone-depleting substances in the atmosphere. *Nat Geosci* 7:266–269.
7. Engel A, et al. (2018) Update on Ozone-Depleting Substances (ODSs) and Other Gases of Interest to the Montreal Protocol, Chapter 1 in *Scientific Assessment of Ozone Depletion: 2018, Global Ozone Research and Monitoring Project — Report No. 58.* (World Meteorological Organisation, Geneva).
8. Prinn RG, et al. (2018) History of chemically and radiatively important atmospheric gases from the Advanced Global Atmospheric Gases Experiment (AGAGE). *Earth Syst. Sci. Data* 10(2):985–1018.
9. Arkema (2016) Proposed closure of the R134a fluorogas activity on the Pierre-Bénite site. https://www.arkema.com/en/media/news/news-details/Proposed-closure-of-the-R134a-fluorogas-activity-on-the-Pierre-Benite-site/, last accessed 12 November 2019.
10. Henne S, et al. (2016) Validation of the Swiss methane emission inventory by atmospheric observations and inverse modelling. *Atmos. Chem. Phys.* 16(6):3683–3710.
11. Rigby M, et al. (2019) Increase in CFC-11 emissions from eastern China based on atmospheric observations. *Nature* 569:546–550.
12. Simmonds PG, et al. (2018) Recent increases in the atmospheric growth rate and emissions of HFC-23 (CHF_3) and the link to HCFC-22 ($CHClF_2$) production. *Atmos. Chem. Phys.* 18(6):4153–4169.
13. Schoenenberger F, et al. (2018) Abundance and sources of atmospheric halocarbons in the Eastern Mediterranean. *Atmos. Chem. Phys.* 18(6):4069–4092.
14. Pisso I, et al. (2019) The Lagrangian particle dispersion model FLEXPART version 10.4. *Geosci. Model Dev.* 12(12):4955–4997.
15. Ruckstuhl AF, et al. (2012) Robust extraction of baseline signal of atmospheric trace species using local regression. *Atmos. Meas. Tech.* 5:2613–2624.
16. Stohl A (1996) Trajectory statistics - a new method to establish source-receptor relationships of air pollutants and its application to the transport of particulate sulfate in Europe. *Atmos. Environ.* 30(4):579–587.
17. Ashbaugh LL, Malm WC, Sadeh WZ (1985) A residence time probability analysis of sulfur concentrations at Grand Canyon National Nark. *Atmos. Environ.* 19(8):1263–1270.